HAL
open science

Gravity-driven migration of one bubble near a free surface: surface tension effects

Marine Guémas, Antoine Sellier, Franck Pigeonneau

▶ To cite this version:

HAL Id: hal-01519296

https://minesparis-psl.hal.science/hal-01519296

Submitted on 6 May 2017

Gravity-driven migration of one bubble near a free surface: surface tension effects

M. Guémas[1], A. Sellier[1] and F.Pigeonneau[2]

[1]LadHyx. Ecole polytechnique, 91128 Palaiseau Cédex, France

[2]Surface du Verre et Interfaces, UMR125 CNRS St Gobain, 39 quai Lucien Lefranc, BP 135, 93303 Aubervilliers, Cedex, France

e-mail: marine.guemas@ladhyx.polytechnique.fr

e-mail: sellier@ladhyx.polytechnique.fr

Abstract We pay attention not only to the time dependant film thickness of the liquid film (so-called drainage) between a bubble and a free surface but also to the bubble and free surface shapes when allowing different uniform surface tensions on these surfaces. This is achieved by extending the recent boundary approach recently employed in [1] for surfaces having identical surface tension. Preliminary numerical results clearly show the sensitivity of the drainage and time-dependent surfaces to the surface tension ratio.3

1. Introduction

Interactions between bubbles and a free surface in a gravity field play a key role in many chemical and geophysical applications. Indeed, as one bubble approaches a free surface, a complex interplay arises between the squeezing of the liquid flow (and film) surrounded by the bubble and the free surface, and the deformations of the aforementioned surfaces shapes. A recent numerical investigation by Pigeonneau and Sellier [1] examined the sensitivity to Bond number (see definition in 2.1) of both the time dependent free surface and bubble(s) shapes and the time dependent film thickness between the free surface and the closest bubble. This was performed for axisymmetric free surface and bubble having the same axis of revolution parallel with the applied gravity field and the *same* uniform surface tension. However, as suggested by a recent paper [2] dealing with the surface tension interaction at the glass-liquid-tin-gas phase interface, the obtained results are very likely to be modified if we consider the case of a free surface and a bubble having *different* (uniform) surface tension $\gamma_0 > 0$ and $\gamma_1 > 0$, respectively. In this work, we therefore extend the study achieved in [1] by considering the case $\gamma_0 \neq \gamma_1$ still resorting to a boundary-integral implementation.

2. Governing problem

2.1 Axisymmetric problem

As sketched in Fig. 1, we consider a bubble B_1 immersed in a Newtonian Fluid with uniform density ρ and viscosity μ bounded by a free surface subject to a uniform gravity $\mathbf{g} = -g\mathbf{e}_z$, with the magnitude g. The ambient fluid above the free surface is a gas with a uniform pressure p_0 and both the temperature T_1 and the pressure p_1 inside the bubble are assumed uniform and constant in time. The bubble surface $S_1(t)$ and the free surface $S_0(t)$ have uniform surface tension $\gamma_1 > 0$ and $\gamma_0 > 0$, respectively. As buoyancy effects drive the bubble toward the free surface, the shape of each surface evolves in time. At initial time, the bubble is taken spherical with radius a and the free surface is the $z = 0$ plane. At any time t, the two deformed bubble surface $S_1(t)$ and free surface $S_0(t)$ are axisymmetric having identical axis of revolution parallel with the gravity $\mathbf{g}$, and the flow in the liquid domain $\mathcal{D}(t)$ has pressure $p + \rho\mathbf{g}.\mathbf{x}$ and velocity $\mathbf{u}$ with typical magnitude $U = \rho g a^2/(3\mu)$. All inertial effect are neglected, i.e the Reynolds number Re obeys Re $= \rho U a/\mu \ll 1$. Assuming quasi-steady bubble and free surface deformations, the flow $(\mathbf{u}, p)$ then satisfies the following far-field behavior and Stokes equations

$$\mu\mathbf{\nabla}^2\mathbf{u} = \mathbf{grad}[p] \; and \; \mathbf{\nabla} \cdot \mathbf{u} = 0 \quad \text{in } \mathcal{D}(t), \; (\mathbf{u}, p) \rightarrow (\mathbf{0}, 0) \quad \text{as} \quad |\mathbf{x}| \rightarrow \infty \tag{1}$$

where $\mathbf{x} = \mathbf{OM}$.

The flow $(\mathbf{u}, p)$ has stress tensor $\boldsymbol{\sigma}$ and, denoting (see Fig.1) by $\mathbf{n}$ the unit normal on $S_0 \cup S_1$ directed
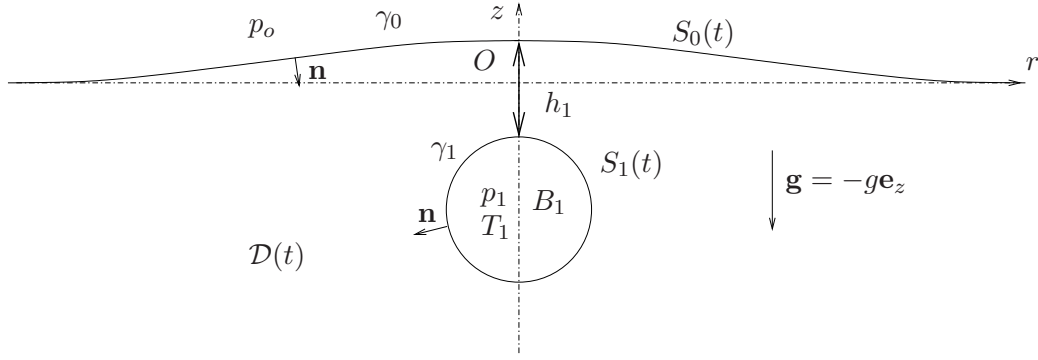

Figure 1: One bubble B_1 ascending near a free surface $S_0(t)$.

into the liquid, one also requires the boundary conditions

$$\boldsymbol{\sigma} \cdot \mathbf{n} = (\rho \mathbf{g} \cdot \mathbf{x} - p_m + \gamma_m \boldsymbol{\nabla}_S \cdot \mathbf{n}) \, \mathbf{n} \text{ on } S_m \text{ for } m = 0, 1 \tag{2}$$

where $[\boldsymbol{\nabla}_S \cdot \mathbf{n}]/2 = H$ is the local average curvature with $[\boldsymbol{\nabla}_S \cdot \mathbf{n}]$, the surface divergence of the unit normal $\mathbf{n}$.

Moreover, there is no mass transfer accross the liquid boundary which implies that

$$\mathbf{V}.\mathbf{n} = \mathbf{u}.\mathbf{n} \text{ on } S_m \text{ for } m = 0, 1 \tag{3}$$

with $\mathbf{V}$ the material velocity on each surface S_m. Finally, since the bubble volume is time-independent, one also requires

$$\int_{S_m} \mathbf{u} \cdot \mathbf{n} dS = 0 \text{ for m=0,1.} \tag{4}$$

To summerize, we represent the time-dependent shape of the free surface and of the bubble by successively running at each time t the following key steps:

i) First, from the knowledge of the surface traction $\boldsymbol{\sigma} \cdot \mathbf{n}$ computed using (2), we solve (1) in conjonction with (4) to obtain the unique solution $\mathbf{u}$ on the surfaces S_0 and S_1.

ii) Then, one calculates the component $\mathbf{V} \cdot \mathbf{n}$ exploiting the relation (3) which allows us to move the surfaces $S_1(t)$ and $S_0(t)$ between time t and time $t + dt$.

2.1 Relevant boundary-integral equations

By virtue of (1)-(2) and (4) the velocity field $\mathbf{u}$ may be computed at any point $\mathbf{x}_0$ located in the liquid domain $\mathcal{D}(t)$ by solely appealing to two surface quantities $\mathbf{u}$ and $\boldsymbol{\sigma} \cdot \mathbf{n}$ on the entire liquid boundary $S = S_0 \cup S_1$. One requires the surface traction $\boldsymbol{\sigma} \cdot \mathbf{n}$ given by the boundary condition (2) to gain the unknown velocity $\mathbf{u}$ on S. This is achieved by letting $\mathbf{x}_0$ tend onto this surface S. Since p_m and γ_m are uniform on each surface S_m, the following boundary-integral equation for the unknown velocity $\mathbf{u}$ on the liquid boundary is then expressed as

$$\mathbf{u}(\mathbf{x}_0) - \frac{1}{4\pi} \int_S \mathbf{u}(\mathbf{x}) \cdot \mathbf{T}(\mathbf{x}, \mathbf{x}_0) \cdot \mathbf{n}(\mathbf{x}) dS = \frac{1}{4\pi\mu} \int_{S_0} [(\rho \mathbf{g} \cdot \mathbf{x} + \gamma_0 \nabla_S \cdot \mathbf{n})\mathbf{n}](\mathbf{x}) \cdot \mathbf{G}(\mathbf{x}, \mathbf{x}_0) dS$$

$$+ \frac{1}{4\pi\mu} \int_{S_1} [(\rho \mathbf{g} \cdot \mathbf{x} + \gamma_1 \nabla_S \cdot \mathbf{n})\mathbf{n}](\mathbf{x}) \cdot \mathbf{G}(\mathbf{x}, \mathbf{x}_0) dS \quad \text{for } \mathbf{x}_0 \text{ on S} \tag{5}$$

where the symbol $\fint$ means a weakly-singular integration in the principal value sense of Cauchy[3] and, setting $x_i = \mathbf{x}.\mathbf{e}_i$ and $x_{0,i} = \mathbf{x}_0.\mathbf{e}_i$, the tensors $\mathbf{G}$ and $\mathbf{T}$ have Cartesian components given by

$$G_{ij}(\mathbf{x}, \mathbf{x}_0) = \frac{\delta_{ij}}{|\mathbf{x} - \mathbf{x}_0|} + \frac{(x_i - x_{0,i})(x_j - x_{0,j})}{|\mathbf{x} - \mathbf{x}_0|^3}, \tag{6}$$

$$T_{ijk}(\mathbf{x}, \mathbf{x}_0) = -6\frac{(x_i - x_{0,i})(x_j - x_{0,j})(x_k - x_{0,k})}{|\mathbf{x} - \mathbf{x}_0|^5}. \tag{7}$$

with δ_{ij} the Kronecker symbol. Since we restrict the analysis to the axisymmetric configuration depicted in Fig.1, we adopt cylindrical coordinates (r, ϕ, z) with $r = \sqrt{x^2 + y^2}$, $z = x_3$ and ϕ the azimuthal angle in the range $[0, 2\pi]$. Setting $\mathbf{u} = u_r \mathbf{e}_r + u_z \mathbf{e}_z = u_\alpha \mathbf{e}_\alpha$ (with $\alpha = r, z$) and $\mathbf{n} = n_r \mathbf{e} + n_z \mathbf{e}_z = n_\alpha \mathbf{e}_\alpha$ on the entire contour $\mathcal{L} = \mathcal{L}_0 \cup \mathcal{L}_1$, with $\mathcal{L}_m$ the trace of the surface S_m integrated over ϕ, then makes it possible to transform (5) as

$$4\pi u_\alpha(\mathbf{x}_0) - \fint_{\mathcal{L}} C_{\alpha\beta}(\mathbf{x}, \mathbf{x}_0)u_\beta(\mathbf{x})dl = -\frac{1}{\mu}\int_{\mathcal{L}_0} B_{\alpha\beta}(\mathbf{x}, \mathbf{x}_0)[-\rho g z + \gamma_0 \nabla_S \cdot \mathbf{n}]n_\beta(\mathbf{x})dl$$

$$-\frac{1}{\mu}\int_{\mathcal{L}_1} B_{\alpha\beta}(\mathbf{x}, \mathbf{x}_0)[-\rho g z + \gamma_1 \nabla_S \cdot \mathbf{n}]n_\beta(\mathbf{x})dl \qquad \text{for } \mathbf{x}_0 \text{ on } \mathcal{L} \tag{8}$$

with $\beta = r$ or $\beta = z$, the differential arc length dl in the $\phi = 0$ plane and the so-called single-layer and double-layer 2×2 square matrices $B_{\alpha\beta}(\mathbf{x}, \mathbf{x}_0)$ and $C_{\alpha\beta}(\mathbf{x}, \mathbf{x}_0)$ given in Pozrikidis [4].

3. Numerical method

In this section, we will briefly introduce the numerical procedure based on a collocation method and a discrete Wiedlandt deflation technique and direct for further details the reader to [1]. The boundary-integral equation (8) is numerically inverted by appealing to the following key steps:

(i) First, a $\mathcal{T}$ truncated free surface contour and the bubble contour are divided into N_e curved boundary elements with the preserved $x \rightarrow -x$ symmetry. Each boundary element has N_c collocation points spread by a Gauss or a uniform distribution. The associated velocity $\mathbf{u}$ and the surface traction $\mathbf{f} = \boldsymbol{\sigma} \cdot \mathbf{n}$ are then approximated on each element using a isoparammetric interpolation. By introducing the components $\mathbf{f}.\mathbf{e}_\alpha$ and $\mathbf{u}.\mathbf{e}_\alpha$ at our $N_e N_c$ nodal points, we end up with two given $2N_e N_c$ stress vector $\mathbf{F}$ and unknown $2N_e N_c$ velocity vector $\mathbf{U}$. Discretizing the boundary-integral equation (8) then shows that these vectors satisfy the $2N_e N_c$-equation linear system

$$\mathbf{U} - \mathbf{C}.\mathbf{U} = \mathbf{B}.\mathbf{F}. \tag{9}$$

The two matrices $\mathbf{B}$ and $\mathbf{C}$ are related to the quantities $B_{\alpha\beta}$ and $C_{\alpha\beta}$ introduced in **2.2** which are integrated on each boundary element by regularizing the weakly-singular terms of $B_{\alpha\alpha}$ when the node $\mathbf{x}_0$ belongs to the selected boundary element.

(ii) By combining (8) and (5), one finds a unique solution $\mathbf{U}$. This solution is here obtained by performing a so-called Wiedlandt's deflation technique to solve (9).

(iii) Note that the major issue for the present work is to precisely calculate the quantity $\nabla_S \cdot \mathbf{n}$ on each discretized surface S_m. An adequate approximation of this quantity indeed dictates the accuracy of the velocity $\mathbf{u}$ calculated through (2) on the fluid boundary. This is achieved by putting enough nodes on each boundary element.

(iv) The shape of each surface S_m is tracked in time using the boundary condition (3) and solving the equation $d\mathbf{x}/dt = \mathbf{u}(\mathbf{x}, t)$ for each nodal point. A Runge-Kutta-Fehlberg method performs this

task using a time-step selected by controlling the errors for the second and third-order schemes. Furthermore, as one shape S_m become nearly time-independent, the adjusted time step is then very small and the computations is stopped.

4. Numerical results

This section presents numerical results for one bubble acsending toward a free surface. First, we look at the dependence of the film thickness h on the z-axis and its sensitivity to the surface tension ratio $r = \gamma_0/\gamma_1$ for a given Bond number $\text{Bo} = \rho g a^2/3\gamma_1$ based on the bubble surface tension. At initial time, the bubble is spherical with radius a and the distance between its center and the flat $z = 0$ free surface is equal to $3a$. Adopting $2a$ as the length scale, the normalized distance between the bubble surface and the free surface is therefore $h_N = h/2a$. Henceforth, t denotes the time normalized by $6\mu/\rho g a$. The numerical implementation is performed taking 45 boundary elements uniformaly spread on the entire contour $\mathcal{L}_1 \cup \mathcal{T}$ and computations are run using 1000 iterations in time. Calculations are stopped whenever the time step selected as explained in section **3**. becomes too small.
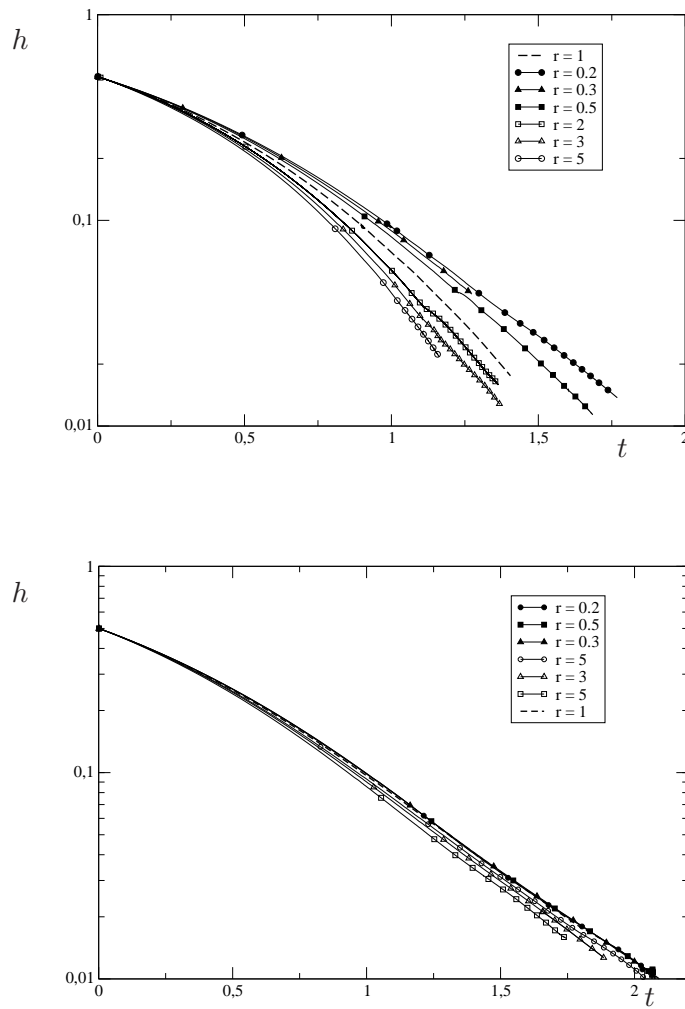

Figure 2: h_N versus t at (a) $\text{Bo} = 0.3$ and (b) $\text{Bo} = 1$ for different values of the surface tension ratio $r = \gamma_0/\gamma_1$.

In order to illustrate the film thickness sensitivity to the surface tension ratio, we plot the evolution in time of the film thickness h_N, for a large range of surface tension ratio γ_0/γ_1 and a given Bond number. As seen in Fig. 2, the film thickness exhibits an exponential decay as time increases whatever

the ratio $r = \gamma_0/\gamma_1$. Observe that at Bo = 0.3 the drainage is significantly enhanced (when compared to the case $\gamma_0 = \gamma_1$) while $\gamma_0 > \gamma_1$ or reduced while $\gamma_0 < \gamma_1$. In contrast, at Bo = 1 the drainage is less sensitive to γ_0/γ_1.
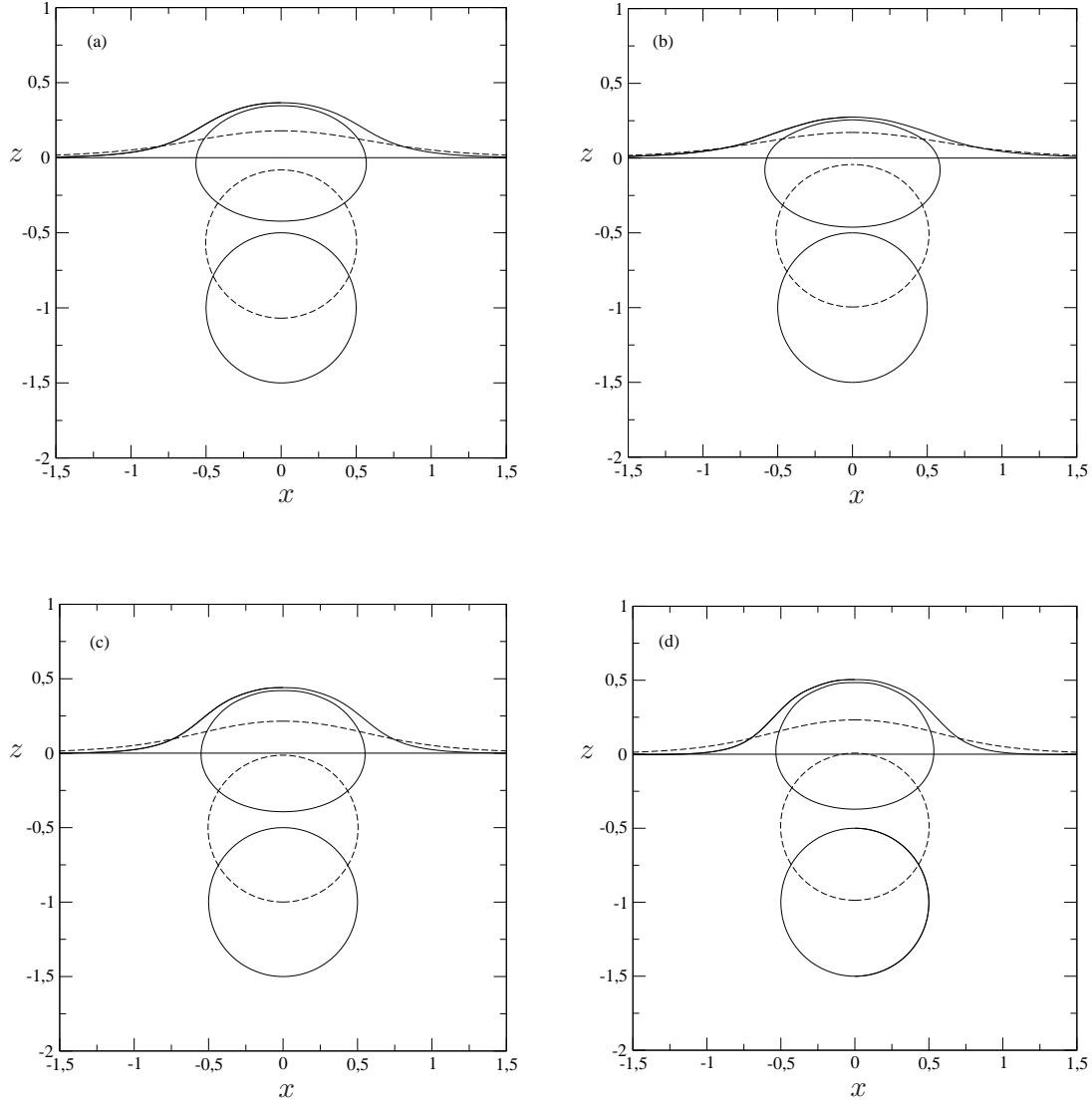

Figure 3: Bubble and free surface shape at Bo = 1 for (a) $\gamma_0/\gamma_1 = 1$, (b) $\gamma_0/\gamma_1 = 2$, (c) $\gamma_0/\gamma_1 = 0.5$ and (d) $\gamma_0/\gamma_1 = 0.2$. Dashed lines indicate the bubble and free surface shapes for $t = 0.59$ while $t = 1.746$ at finale stage.

Fig. 3 depicts the time-dependent bubble and free surface shapes sensitivity to the surface tension ratio. Note that the free surface is slightly less deformed when $\gamma_0/\gamma_1 = 2$ (Fig. 3 (b)) than when $\gamma_0 = \gamma_1$ (Fig. 3 (a)). This explains why, in Fig. 2 the drainage is indeed enhanced for $\gamma_0/\gamma_1 > 1$. When $\gamma_0 < \gamma_1$, though the drainage observed in Fig. 2 (b) are closely identical for $\gamma_0/\gamma_1 = 0.5$ and $\gamma_0/\gamma_1 = 0.2$, the final free surface shapes shown Fig. 3 (c) and Fig. 3 (d) are slightly different.

5. Conclusions

Our investigations reveal that both the drainage and the time-dependent shapes of the bubble and free surface depend upon the surface tension ratio γ_0/γ_1. Additional numerical results will be reported and discussed at the oral presentation. Finally, one should note that the proposed boundary-integral

approache is also able to deal with several bubbles.

References

[1] F. Pigeonneau and A. Sellier. Low-Reynolds-Number gravity-driven migration and deformation of bubbles near a free surface. *Phys. Fluids*, 23:092302, 2011.

[2] V. I. Nizhenko and Yu. I. Smirnov Surface Phenomena and interfacial interaction at the glass-liquid tin-gas phase interface. *Powder Metallurgy and Metal Ceramics*, 42:075084, 2003.

[3] J. Hadamard Lecture on Cauchy's problem in linear differential equations, Dover Publications, Inc., New York, 1932.

[4] C. Pozrikidis Boundary integral and singularity methods for linearized viscous flow. Cambridge University Press, 1992.